Adaptive Two-Step Peer Methods for Incompressible Navier-Stokes Equations

Bettina Gottermeier*, Jens Lang
*gottermeier@mathematik.tu-darmstadt.de

TECHNISCHE UNIVERSITÄT DARMSTADT

Research Group
Numerical Analysis and
Scientific Computing

Abstract

The paper presents a numerical study of two-step peer methods up to order six, applied to the non-stationary incompressible Navier-Stokes equations. These linearly implicit methods show good stability properties, but the main advantage over one-step methods lies in the fact that even for PDEs no order reduction is observed. To investigate whether the higher order of convergence of the two-step peer methods equipped with variable time steps pays off in practically relevant CFD computations, we consider typical benchmark problems. Higher accuracy and better efficiency of the two-step peer methods compared to classical third-order one-step methods of Rosenbrock-type can be observed.

1 Introduction

In industrial and scientific applications, incompressible flows are modelled by the well-known Navier-Stokes equations, for which the time-dependent system on the domain $[0,T]\times\Omega, \Omega\subset\mathbb{R}^2$ is given by the following nonlinear equations

$$\partial_t u - Re^{-1}\Delta u + (u\cdot\nabla)u + \nabla p = F \qquad \text{in } (0,T]\times\Omega \tag{1.1a}$$
$$\nabla\cdot u = 0 \qquad \text{in } [0,T]\times\Omega \tag{1.1b}$$
$$u = G \qquad \text{on } [0,T]\times\partial\Omega \tag{1.1c}$$
$$u(0,x) = u_0 \qquad x\in\Omega\,. \tag{1.1d}$$

The vector $u=(u_1,u_2)^T\in\mathbb{R}^2$ represents the velocity field, the scalar p the pressure function and F denotes external forces. The Reynolds number Re will be limited to laminar flows in this paper. The function G and u_0 are given by boundary and initial conditions, respectively.

In recent time, intensive research on numerical methods has been made for an accurate and efficient numerical solution of the Navier-Stokes equations. Unfortunately, classical one-step methods, such as Runge-Kutta and Rosenbrock methods, suffer from order reduction when they are applied to partial differential equations (PDEs). In this paper, linearly implicit two-step peer methods are used to solve the nonlinear Navier-Stokes equations. There exists methods up to order six, which provide good stability properties, i.e., $L(\alpha)$-stability with an angle α of at least 85°. Because of the embedding of the Jacobian matrix directly into the integration formula, they require only the solution of linear systems in each time step, making them very attractive for practical computations. The main advantage over one-step methods lies in the fact that even the higher-order peer methods have shown no order reduction when they are applied to PDEs. Additionally, they are competitive compared to the applied one-step methods and sometimes even more efficient [2].

The present paper is organized as follows: In Sect. 2 we begin with the time and space discretizations of the Navier-Stokes equations and explain the strategy for the time adaptivity in KARDOS [1], the finite element software package used for the numerical computations. Results of the numerical simulations are contained in Sect. 3. An analytical example to validate the higher orders of convergence as well as a typical benchmark problem is presented. Finally, we summarize our results and conclusions in Sect. 4.

2 Discretization of the Navier-Stokes Equations

For a higher-order temporal discretization of the instationary Navier-Stokes equations, we apply an s-stage linearly implicit two-step peer method [2] to (1.1).

Let $\tau_m > 0$ be a variable time step and $V_{mi} = (P_{mi}, U_{mi})^T$ the approximation to the exact solution at time $t_{mi} := t_m + c_i\tau_m$ with $t_m = t_{m-1,s}$ for $m \geq 1$ and $c_i \in [-1,1]$, $c_s = 1$. Then the system of linear equations which has to be solved for each time step reads as

$$\left(\frac{I}{\tau_m\gamma} - Re^{-1}\Delta + U_{m-1,s}\cdot\nabla\right)(U_{mi} - U^0_{mi}) + ((U_{mi} - U^0_{mi})\cdot\nabla)U_{m-1,s} + \nabla(P_{mi} - P^0_{mi})$$
$$= (Re^{-1}\Delta - (U^0_{mi}\cdot\nabla))U^0_{mi} - \nabla P^0_{mi} + \frac{1}{\tau_m\gamma}(Qw_i - U^0_{mi}) + F(t_{mi}) \tag{2.2a}$$
$$\nabla\cdot(U_{mi} - U^0_{mi}) = -\nabla\cdot U^0_{mi} \tag{2.2b}$$

for $i = 1,...,s$, with the boundary conditions $U_{mi} = G(t_{mi})$. The internal values and the predictors are given by

$$w_i = \sum_{j=1}^{i-1}\frac{1}{\gamma}a_{ij}(V_{mj} - w_j) + \sum_{j=1}^{s}u_{ij}(\sigma_m)V_{m-1,j}\,,$$
$$V^0_{mi} = \sum_{j=1}^{i-1}\frac{1}{\gamma}a^0_{ij}(V_{mj} - w_j) + \sum_{j=1}^{s}u^0_{ij}(\sigma_m)V_{m-1,j}\,.$$

The matrix Q is defined such that only the second component of the vector w_i is selected. The values for the abscissa $c \in \mathbb{R}^s$ are stretched Chebychev nodes

$$c_i := -\frac{\cos\left(\left(i - \frac{1}{2}\right)\frac{\pi}{s}\right)}{\cos\left(\frac{\pi}{2s}\right)}\,, \quad i = 1,...,s$$

with $c_s = 1$. The remaining coefficients of the method are combined in a lower triangular matrix $A = (a_{ij}) \in \mathbb{R}^{s\times s}$ with constant diagonal elements $a_{ii} = \gamma > 0$ and in a possibly full matrix $U = (u_{ij}) \in \mathbb{R}^{s\times s}$ which depends on the step size ratio $\sigma_m := \tau_m/\tau_{m-1}$. For the predictor V^0_{mi}, the real coefficient matrices have similar properties:

$$A^0 = (a^0_{ij}) \quad \text{with} \quad a^0_{ij} = 0 \quad \text{for} \quad i \leq j \quad \text{and} \quad U^0 = (u^0_{ij}(\sigma_m))\,.$$

The coefficients are chosen in such a way that the method has order $p = s$ for constant step size and order $p = s - 1$ for variable step size.

Adaptivity in time is gained with an embedding strategy. A second solution $\tilde{V}_{ms}$ of inferior order $\tilde{p} = s - 2$ is computed by a linear combination of the V_{mi}, $i = 1,...,s-1$. The new time step size is then defined by

$$\tau_{\text{new}} = \min\{\tau_{\max}, \min\{2, \max\{0.2, (TOL_t/ERR_t)^{1/(\tilde{p}+1)}\}\}\times 0.9\tau_m\}\,,$$

where

$$ERR_t := \left(\frac{1}{n}\sum_{i=1}^{n}\frac{\|V_{ms} - \tilde{V}_{ms}\|^2_{L_2}}{\left(ScalR_i\,\|e_i^T V_{ms}\|_{L_2} + ScalA_i\sqrt{|\Omega|}\right)^2}\right)^{\frac{1}{2}}$$

and $ScalR_i$, $ScalA_i$ and TOL_t are user-prescribed parameters for the relative and absolute scaling factors and the desired time tolerance, respectively. For a more detailed description we refer to [2].

In the next step, the arising spatial problems (2.2), now independent of time, are solved by a multilevel finite element method [5]. We select finite dimensional subspaces S^q_h of the finite element meshes $\mathcal{T}^h_m$ at

time $t = t_m$ with refinement level h, where the continuous functions of S_h^q are chosen to be polynomials of order q on each finite element $T \in \mathscr{T}_m^h$. Defining $\hat{P}_{mi} = P_{mi} - P_{mi}^0$ and $\hat{U}_{mi} = U_{mi} - U_{mi}^0$, the standard Galerkin finite element solutions $V_{mi}^h \in S_h^q$ can then be computed from the equations

$$\begin{aligned}\frac{I}{\tau_m \gamma}\left(\hat{U}_{mi}^h, \varphi\right) - Re^{-1}\left(\Delta \hat{U}_{mi}^h, \varphi\right) + \left((U_{m-1,s} \cdot \nabla)\hat{U}_{mi}^h, \varphi\right) + \left((\hat{U}_{mi}^h \cdot \nabla)U_{m-1,s}, \varphi\right) + \left(\nabla \hat{P}_{mi}^h, \varphi\right) \\ = \left(\hat{F}^h(t_{mi}, P_{mi}^{0,h}, U_{mi}^{0,h}), \varphi\right) \\ \left(\nabla \cdot \hat{U}_{mi}^h, \varphi\right) = -\left(\nabla \cdot U_{mi}^{0,h}, \varphi\right), \quad \forall \varphi \in S_h^q,\end{aligned}$$

where $\hat{F}^h(t_{mi}, P_{mi}^{0,h}, U_{mi}^{0,h})$ is the right hand side of equation (2.2a). Because of numerical oscillations in V_{mi}^h due to advection-dominated terms, we choose a Galerkin/least-squares method to stabilize the discretization by adding locally weighted residuals as described in [5]. We use the same finite element functions for the pressure and the velocity. To avoid spurious pressure modes of the numerical solution, a relaxation of the incompressibility condition

$$\nabla \cdot u = \delta \nabla \cdot \left(\partial_t u - Re^{-1}\Delta u + (u \cdot \nabla)u + \nabla p - F\right)$$

is applied to get a stable discretization, where δ is defined by

$$\delta = c\frac{h_b}{2u_{\text{ref}}}\frac{\hat{Re}}{\sqrt{1+\hat{Re}^2}}, \quad \hat{Re} = h_b u_{\text{ref}} Re, \quad c = 0.4,$$

with a global reference velocity u_{ref} and the diameter h_b of the two-dimensional ball which is area-equivalent to the element $T \in \mathscr{T}^h$.

3 Numerical Results

We first apply the two-step methods PEER4, PEER5 and PEER6 [2] to (1.1) with given analytical solution to validate their classical orders 4, 5 and 6, respectively. Then, a typical benchmark problem is considered to study the accuracy and efficiency of these methods equipped with variable time steps. Comparisons are made with linearly implicit one-step Rosenbrock methods ROS3P [7] and ROS3PL [6] of classical order three.

3.1 Analytical Example

We choose a very stiff test case [4], where the computational domain is chosen to be the unit square $\Omega = (0,1)^2$, the final time is T and the Reynolds number Re is set to 1. The functions F, G and u_0 in (1.1) are computed with the help of the exact solution

$$\begin{aligned}p(t,x,y) &= (10+t)e^{-t}(x+y-1)\\ u_1(t,x,y) &= t^3 y^2\\ u_2(t,x,y) &= e^{-50t}x\,.\end{aligned}$$

We implement Dirichlet boundary conditions and use a quadratic ansatz for the finite elements on a fixed spatial mesh consisting of 2048 triangles. In this way, the spatial discretization is solved exactly and the arising errors consist of the time integration errors only.

We consider the global error for the solution vector $v = (p, u_1, u_2)^T$ in the norm $L^2(0,1;L^2(\Omega))$, i.e.,

$$\|v - v_h\|_{L^2(0,1;L^2(\Omega))} = \left(\int_0^1 \|v - v_h\|_{L^2(\Omega)}^2 dt\right)^{1/2}.$$

The simulations are performed with fixed and variable time steps and starting values taken from the exact solution.

3.1.1 Validation of Higher Orders of Convergence

Fixed time steps are chosen to validate the higher orders of convergence of the tested methods. The global errors for the two-step peer methods as well as for the one-step Rosenbrock solvers are presented in Fig. 1 for several numbers of time steps. The peer methods achieve their higher orders and show the super-convergence property. Likewise, the one-step Rosenbrock solvers show order three as expected. The advantage of the peer methods becomes obvious not only because of the higher order of convergence but also when considering the computed errors. At least one order of magnitude for each time step size can be gained choosing a method with a higher order.

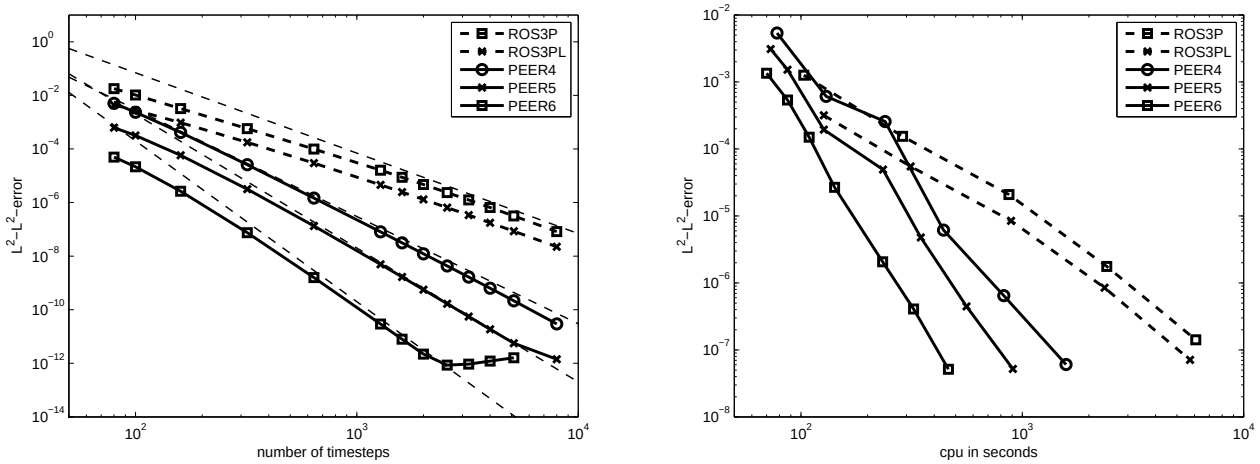

Figure 1: In the left picture, where the computed error is drawn against the number of timesteps, the expected order can be observed for peer and Rosenbrock solvers. The picture on the right shows the higher efficiency of the two-step methods compared to the tested one-step methods. The requested time tolerances are $10^{-i}, i = 0, \ldots, 6$.

3.1.2 Efficiency

Time-adaptive simulations are considered to show the good performance of the peer methods compared to the tested Rosenbrock solvers. The requested time tolerances are set to 10^{-i}, $i = 0, \ldots, 6$, and the new time step is chosen according to the adaptive strategy in Sect. 2. The results are shown in the right picture of Fig. 1, where the global error is drawn against CPU time in seconds. The higher efficiency of the peer methods compared to the Rosenbrock methods can be observed clearly, especially for more stringent time tolerances. Considering shorter CPU times the two-step methods are still comparable with the one-step Rosenbrock solvers.

3.2 Flow Around a Cylinder

We consider the benchmark problem of a laminar flow around a cylinder in two dimensions, which was defined within the DFG Priority Research Programme "Flow Simulation on High Performance Computers" [8]. We choose the third case therein, which uses the instationary Navier-Stokes equations (1.1) combined with a time-dependent parabolic inflow profile

$$u_1(t, 0, y) = 4u_m y(H - y)\sin(\pi t/8)/H^2\,, \quad u_2 = 0$$

with $u_m = 1.5\,\mathrm{m/s}$ in the time interval $0 \le t \le 8\,\mathrm{s}$. The computational domain Ω is shown in Fig. 2 with $H = 0.41\,\mathrm{m}$ and the diameter $D = 0.1\,\mathrm{m}$ of the cylinder. The characteristic values of the fluid are the

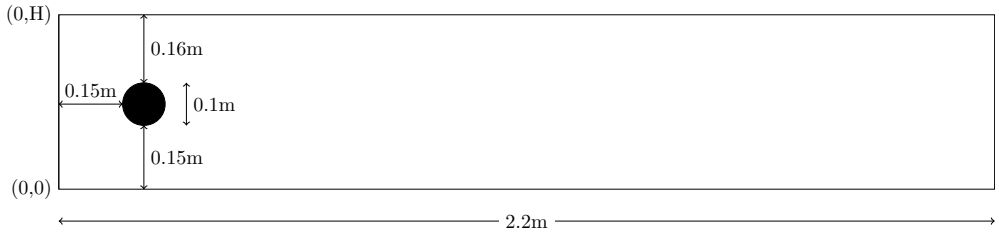

Figure 2: Computational domain Ω.

kinematic viscosity $\nu = 10^{-3}\,\mathrm{m}^2/\mathrm{s}$ and the density $\varrho = 1.0\,\mathrm{kg/m}^3$. The time-dependent Reynolds number is defined by $Re = \bar{u}D/\nu$ with mean velocity $\bar{u} = 2u_{\max}/3 = 2u(t,0,H/2)/3$ yielding values in the interval $[0,100]$.

The initial conditions are $u_1 = u_2 = 0$. For the velocity vector, we prescribe the given parabolic inflow profile for $x = 0$ and a non-flux boundary condition for $x = 2.2$. On all remaining parts, no-slip boundary conditions are imposed.

The performance of the different solvers which are applied to the benchmark problem are compared by means of the drag and lift coefficients as well as the pressure difference between the front and the back of the cylinder

$$\Delta p(t) = p(t,0.15,0.2) - p(t,0.25,0.2)\,.$$

We use a volume integral formulation for the drag and lift coefficients

$$c_d(t) = -k\int_\Omega \left[\partial_t u(t)\cdot v_d + \nu\nabla u(t) : \nabla v_d + (u(t)\cdot\nabla)u(t)\cdot v_d - p(t)(\nabla\cdot v_d)\right] dxdy\,,$$
$$c_l(t) = -k\int_\Omega \left[\partial_t u(t)\cdot v_l + \nu\nabla u(t) : \nabla v_l + (u(t)\cdot\nabla)u(t)\cdot v_l - p(t)(\nabla\cdot v_l)\right] dxdy\,,$$

$k := 2/(\varrho D u_{\max}^2)$, as these seem to be more accurate and less susceptible to approximations of the cylinder boundary than a line integral formulation [3]. The formulas are valid for all functions $v_d, v_l \in (H^1(\Omega))^2$ with $(v_d)|_S = (1,0)^T, (v_l)|_S = (0,1)^T$ on the cylinder boundary S and vanishing v_d, v_l on all other boundaries. We take the maximal values for the drag and lift coefficients in the time interval $[0,T]$ and the pressure difference at the final time $T = 8\,\mathrm{s}$ and compare them with the following reference values:

$$c_{d,\max} = 2.952003\,, \qquad c_{l,\max} = 0.4773925\,, \qquad \Delta p = -0.1116111\,.$$

These values lie in the intervals computed in [8] and are comparable to the ones obtained in [3].

A very fine mesh, particularly at the cylinder boundary, which consists of 119918 triangles, is used because of the sensitivity of the lift coefficient to the discretization in space. Linear finite elements are chosen to perform the time-adaptive simulations.

The good performance of the two-step peer methods compared to the one-step methods can be observed in Fig. 3 considering CPU times needed for comparable accuracy. The peer methods, in particular Peer5, are highly accurate and much more efficient than the tested one-step methods Ros3p and Ros3pl.

4 Conclusions

We have applied linearly implicit two-step peer methods and a multilevel finite element method based on a Galerkin/least-squares stabilization to solve the non-stationary incompressible Navier-Stokes equations. The two-step methods have shown their expected classical orders of convergence and even the

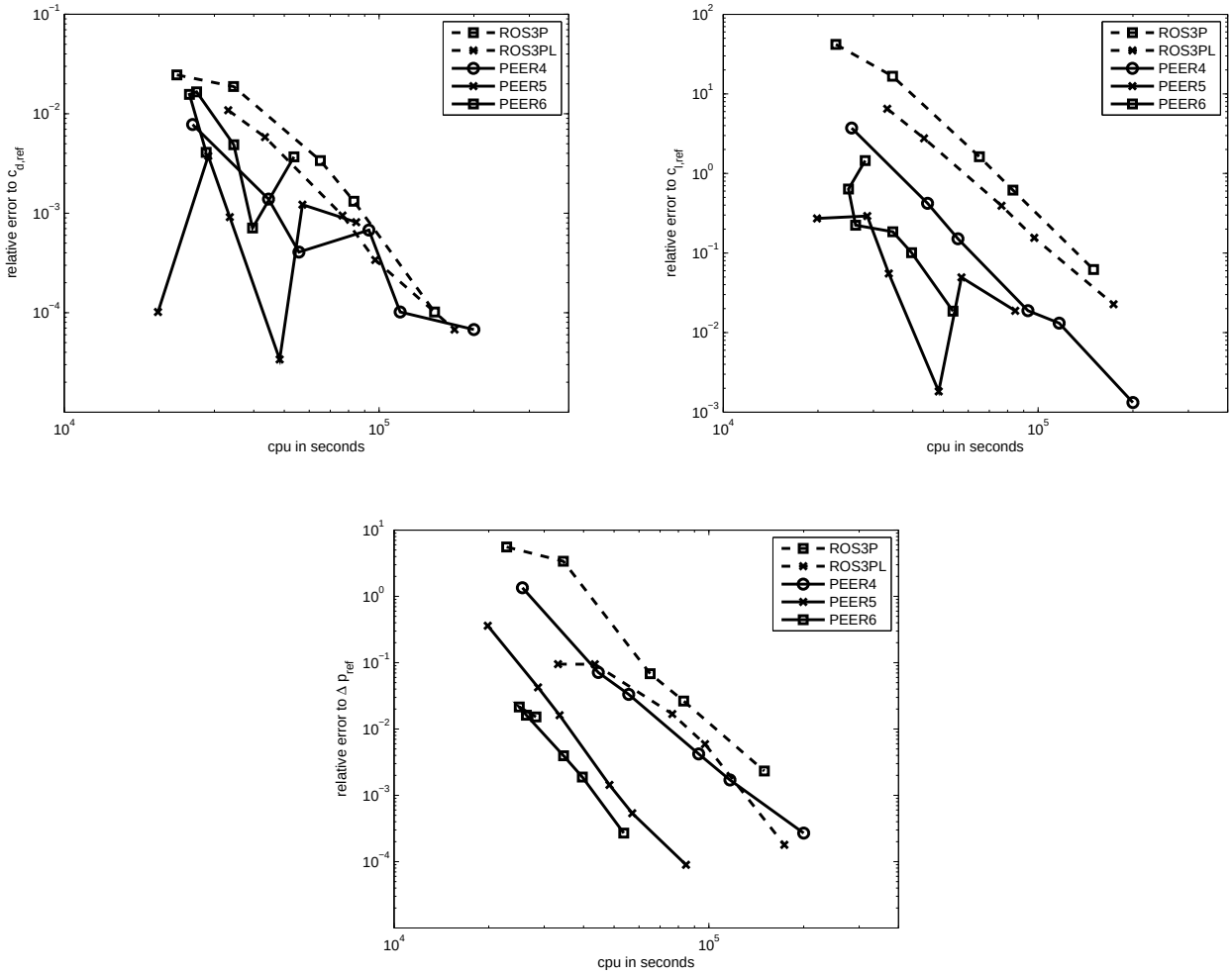

Figure 3: Relative error of drag (top left) and lift (top right) coefficients and pressure difference (bottom) for peer and Rosenbrock solvers. The requested time tolerances are $5 \times 10^{-3}, 10^{-3}, \ldots, 10^{-5}$ for the peer methods and $10^{-4}, 5 \times 10^{-5}, \ldots, 10^{-6}$ for the Rosenbrock methods.

super-convergence property can be observed. Compared to Rosenbrock-type one-step methods, the peer methods are more accurate and provide an efficient solution for incompressible flows.

Bibliography

[1] Erdmann, B., Lang, J., Roitzsch, R.: KARDOS user's guide. Tech. Rep. ZR 02–42, Konrad-Zuse-Zentrum Berlin, 2002

[2] Gerish, A., Lang, J., Podhaisky, H., Weiner, R.: High-order linearly implicit two-step peer–finite element methods for time-dependent PDEs. Appl. Numer. Math **59**, 624–638 (2009)

[3] John, V.: Reference values for drag and lift of a two-dimensional time-dependent flow around a cylinder. Int. J. Numer. Meth. Fluids **44**, 777–788 (2004)

[4] John, V., Matthies, G., Rang, J.: A comparison of time-discretization / linearization approaches for the incompressible Navier-Stokes equations. Tech. Rep. 353, Ruhr-Universität Bochum, 2004

[5] Lang, J.: Adaptive incompressible flow computations with linearly implicit time discretization and stabilized finite elements. In: Papailiou, K.D., Tsahalis, D., Periaux, J., Hirsch, C., Pandolfi, M. (eds.) Computational Fluid Dynamics, pp. 200–204. John Wiley & Sons, New York (1998)

[6] Lang, J., Teleaga, D.: Towards a fully space-time adaptive FEM for magnetoquasistatics. IEEE Trans. Magn. **44**, 1238–1241 (2008)

[7] Lang, J., Verwer, J.: ROS3P—an accurate third-order Rosenbrock solver designed for parabolic problems. BIT **41**, 731–738 (2001)

[8] Schäfer, M., Turek, S.: Benchmark computations of laminar flow around a cylinder. In: Hirschel, E.H. (ed.) Flow Simulation with High-Performance Computers II, pp. 547–566. Vieweg (1996)